

Tuning the Topological Features of Quantum-Dot Hydrogen and Helium by a Magnetic Field

Wenchen Luo

*School of Physics and Electronics, Central South University, Changsha, Hunan, P. R. China 410083 and
Department of Physics and Astronomy, University of Manitoba, Winnipeg, Canada R3T 2N2*

Tapash Chakraborty*

Department of Physics and Astronomy, University of Manitoba, Winnipeg, Canada R3T 2N2

(Dated: August 20, 2019)

The topological charge of the spin texture in a quantum dot with spin-orbit couplings is shown analytically here to be stable against the ellipticity of the dot. It is directly tunable by a single magnetic field and is related to the *sign* of the Landé g factor. In a quantum-dot helium, the overall winding number could have different property from that of the single-electron case (quantum-dot hydrogen), since tuning the number of electron affects the winding number by the Coulomb interaction and the z component angular momentum ($\langle L_z \rangle$). The density profile and the spin texture influence each other when the Coulomb interaction is present. When $\langle L_z \rangle$ is biased away from an integer by the spin-orbit couplings, the rotational symmetry is broken which induces strong density deformation. The sign of the topological charge may also be reversed with increasing magnetic field. These findings are of major significance since the applied magnetic field alone now provides a direct route to control the topological properties of quantum dots.

I. INTRODUCTION

Studies of topological spin textures have made great strides in condensed matter physics¹. The important role of spin-orbit coupling (SOC) has been brought to the fore, in particular, since the discovery of the topological insulator^{2,3}. It also plays a crucial role in various topological states in nanoscale quantum systems. Basically, there are two important concepts that govern the topological properties of the states. One is that in momentum space the band structures are topologically non-trivial, such as topological insulators and topological superconductors. The other is that the states contain topologically non-trivial structures in real space, such as helical magnets^{4,5}, skyrmions in quantum Hall regime^{6,7}, skyrmion lattice in non-interacting two sub-band GaAs quantum well⁸ etc. The topological band structure is able to introduce special transport phenomena, while the topological electron states in real space induced by the SOCs would be important for spintronics and quantum information applications⁹⁻¹¹. We have recently found¹² that the spin fields are vortices in a quantum dot (QD) ('artificial atom')¹³⁻¹⁸ in the presence of SOCs¹⁹⁻³⁶, mostly at the single-electron level. The vortices in real space apparently appear due to the confinement induced translational symmetry breaking. The topological features are distinguished by the competition of the two SOCs: the topological charge of the spin field is 1 when the Rashba SOC is much stronger than the Dresselhaus SOC; and -1 when the Dresselhaus SOC dominates the system in a weak magnetic field (e.g., $B \ll 1\text{T}$).

In this work, we mainly focus on how the effects of the Coulomb interaction and a single magnetic field change the topological properties of the spin of the electrons in quantum dots. In addition, comparison between the many-body states and the single-electron state is neces-

sary for that purpose. In order to be clearer about the topological properties of the system, we introduce the winding number to describe the topological charge of the spin field conveniently. So we can analytically study the spin textures with different SOCs and magnetic fields. Particularly, we prove analytically that the topological charge is robust against the deformation of the shape of the quantum dot, and is tunable in a single magnetic field.

For the single electron case, by employing the perturbation theory in terms of the magnetic field strength and the SOCs, we show that the inversion of the topological charge, when both of the Rashba and the Dresselhaus SOCs exist, is even controllable by a single magnetic field. We further show that the topological charge of the spin field with increasing of the magnetic field has the opposite sign of the Landé g factor, irrespective of the single-electron or many-electron states. We note that the perturbation theory is valid in an arbitrarily large magnetic field, since the perturbation terms always have smaller energy scales than that of the unperturbative one.

In order to study the interacting system, we concentrate on the two-electron QD for simplicity, namely the QD helium^{37,38}. We numerically calculate the energy spectrum and the many-particle wave functions of the QD helium, by the method of exact diagonalization. We consider the variation of the expectation values of the z component of the angular momentum and the spin, $\langle L_z \rangle$ and $\langle \sigma_z \rangle$ respectively, versus the magnetic field, in analogy to the phase transition theory. However, as the system size is finite and no thermodynamic limit is possible, we only mention about *transitions of these quantities*. For instance, if the curve of $\langle L_z \rangle(B)$ ($\langle \sigma_z \rangle(B)$) is not differentiable, then the discontinuous transitions occur (akin to first-order transitions). If this curve is differentiable, but with some clear plateaus develop, then

the smooth transitions occur (similar to a change to a second-order transition).

If there is no SOC in such a system, the spin field would be trivial, only the z component of the spin exists, and $\langle L_z \rangle$ is quantized with increasing of the magnetic field. In fact, the SOCs are able to turn the transition of L_z to second order even in an isotropic dot, as L_z does not commute with the SOCs. The rotational symmetry of the density may be broken when $\langle L_z \rangle$ is no longer an integer. The system becomes even more interesting if both spin and density are controlled by the magnetic field or the electric field (Rashba SOC is tuned by the electric field³⁹⁻⁴³). We thus report here how the combination of the Coulomb interaction, Rashba and Dresselhaus SOCs modify the spin textures of these systems. Since the density profile and the spin textures are closely dependent on and influence each other, we also study the evolution of both density and spin with the magnetic field.

We further explore the relations between the topological charge of the spin field and $\langle L_z \rangle$ or $\langle \sigma_z \rangle$, which is controlled by the external magnetic field. Quite remarkably, since the topological features are directly tunable by the Landé g factor and the number of electrons in our present approach, the sign of the Landé g factor which is difficult to determine experimentally⁴⁴ may be addressed by detecting the topological features of the electrons properly.

The manuscript is organized as follows. In Section II, we introduce the Hamiltonians of the QD hydrogen and the QD helium, and explicitly express the winding number to define the topological charge of the in-plane spin field. We write down the definition of the spin fields and the density which will be studied in details in the following sections. Then we demonstrate that the topological charge is robust against the ellipticity of the dots in Section III. We also derive the topological charge to have the opposite sign of the Landé g factor in strong magnetic fields, which can be verified numerically. In Section IV, we consider an InAs and a ZnO QD helium. We study how the spin texture and the density distribution of the electrons involves with increasing of the magnetic field. Then we study the relation among spin fields, $\langle L_z \rangle$, $\langle \sigma_z \rangle$, and the Coulomb interaction on the topological charge of the system particularly. Finally, we conclude this work.

II. THE HAMILTONIAN AND THE WINDING NUMBER OF THE SPIN FIELD

The single-electron Hamiltonian in a QD with SOCs is

$$\mathcal{H} = \frac{\mathbf{P}^2}{2m^*} + \frac{m^*}{2} (\omega_x^2 x^2 + \omega_y^2 y^2) + \frac{\Delta}{2} \sigma_z + \mathcal{H}_{SOC}, \quad (1)$$

$$\mathcal{H}_{SOC} = g_1 (\sigma_x P_y - \sigma_y P_x) + g_2 (\sigma_y P_y - \sigma_x P_x), \quad (2)$$

where ω_x and ω_y describe the parabolic confinements in x and y direction, respectively. σ_i is the Pauli matrix and the strengths of the Rashba and Dresselhaus SOCs are g_1 and g_2 respectively. $P_i = p_i + eA_i$ is the kinetic

momentum. The vector potential is chosen to be in the symmetric gauge $\mathbf{A} = \frac{1}{2}B(-y, x, 0)$ with the magnetic field B . The Zeeman coupling is then $\Delta = g\mu_B B$, where g is the Landé factor. In fact, we can rewrite the Hamiltonian in the form of

$$\mathcal{H} = \mathcal{H}_0 + \mathcal{H}_{L_z} + \mathcal{H}_{SOC}, \quad (3)$$

$$\mathcal{H}_0 = \frac{\mathbf{P}^2}{2m^*} + \frac{m^*}{2} (\Omega_x^2 x^2 + \Omega_y^2 y^2) + \frac{\Delta}{2} \sigma_z, \quad (4)$$

$$\mathcal{H}_{L_z} = \frac{eB}{2m^*} (xp_y - yp_x), \quad (5)$$

where \mathcal{H}_0 describes a two-dimensional harmonic oscillator, and \mathcal{H}_{L_z} is proportional to the z -component of the angular momentum L_z . In the following perturbative calculations, \mathcal{H}_0 is the unperturbed Hamiltonian, and its eigenvectors are chosen to be the basis in the numerical exact diagonalizations. We introduce the frequencies $\Omega_{x,y} = \sqrt{\omega_{x,y}^2 + \omega_c^2/4}$ with the anisotropic confinement frequencies in two directions, and the cyclotron frequency $\omega_c = eB/m^*$. The confinement lengths are $R_i = \sqrt{\hbar/(m^*\omega_i)}$, and the natural length are $\ell_i = \sqrt{\hbar/(m^*\Omega_i)}$. The eigen state of the harmonic oscillator with its eigen wavefunction $\psi_{n_x, n_y}(\mathbf{r})$, where $n_{x,y}$ are the quantum numbers of the oscillator, is used as the basis of the calculations.

If there are more than one electrons in the QD, we need to take the Coulomb interaction into account, which can be written, in the second quantization,^{12,14,24,27}

$$\mathcal{H}_C = \frac{1}{2} \sum_{i,j,k,l} \sum_{s,s'} V_{i,j,k,l} c_{i,s}^\dagger c_{j,s'}^\dagger c_{k,s'} c_{l,s}, \quad (6)$$

where c is the operator of an electron, s, s' are the spin indices, i, j, k, l stand for the combination indices which contains the x, y quantum numbers of the oscillator. For example, $k = (k_x, k_y)$, $k_{x,y}$ are the quantum numbers of the oscillator in x and y directions, respectively. The Coulomb interaction matrix element $V_{i,j,k,l}$ is calculated numerically by a two-dimensional integral,

$$V_{i,j,k,l} = \frac{2}{\pi} \frac{e^2}{\epsilon \sqrt{\ell_x \ell_y}} (-1)^{|j_x - k_x| + |j_y - k_y|} \quad (7)$$

$$\gamma(i_x, l_x) \gamma(i_y, l_y) \gamma(j_x, k_x) \gamma(j_y, k_y)$$

$$i^{|i_x - l_x| + |i_y - l_y| + |j_x - k_x| + |j_y - k_y|}$$

$$\int dx dy \Phi(i_x, l_x, x) \Phi(j_x, k_x, x) \frac{\Phi(i_y, l_y, y) \Phi(j_y, k_y, y)}{\sqrt{\frac{\ell_y}{\ell_x} x^2 + \frac{\ell_x}{\ell_y} y^2}},$$

where ϵ is the dielectric constant and

$$\gamma(n, m) = \sqrt{\frac{2^{\min(n,m)} \min(n, m)!}{2^{\max(n,m)} \max(n, m)!}}, \quad (8)$$

$$\Phi(n, m, x) = x^{|n-m|} e^{-\frac{1}{4}x^2} L_{\min(n,m)}^{|n-m|} \left(\frac{x^2}{2} \right) \quad (9)$$

with the Laguerre polynomial L . We note that the integrand is even ($|i_x - l_x| + |i_y - l_y| + |j_x - k_x| + |j_y - k_y|$ is even), otherwise the integral would be zero, which guarantees the Coulomb interaction matrix element to be real.

We then exactly diagonalize the total Hamiltonian $\mathcal{H}_T = \mathcal{H} + \mathcal{H}_C$ to obtain the wave function of the state that we would like to study. The selected state is supposed to be

$$|\Psi\rangle = \sum_{\{j\}} d_j |(j_1, s_1), (j_2, s_2), \dots, (j_{N_e}, s_{N_e})\rangle, \quad (10)$$

where N_e is the electron number and d_j is the coefficient of the many-particle (or a single-particle) basis obtained by the exact diagonalization. In the many-particle state $|(j_1, s_1), (j_2, s_2), \dots, (j_{N_e}, s_{N_e})\rangle$, (j_n, s_n) are the indices for the n -th electron of the system, where j_n is the combination index containing the x, y quantum numbers of the oscillator and s_n is the spin index. The spin fields $\sigma_\mu(\mathbf{r})$ of such a state can be defined generally by

$$\begin{aligned} \sigma_\mu(\mathbf{r}) &= \sum_{\{i\}, \{j\}} d_i^* d_j \sum_{k, l, s, s'} \psi_{k, s}^\dagger(\mathbf{r}) \sigma_\mu \psi_{l, s'}(\mathbf{r}) \\ &\langle (i_1, s'_1), \dots, (i_{N_e}, s'_{N_e}) | c_{k, s}^\dagger c_{l, s'} | (j_1, s_1), \dots, (j_{N_e}, s_{N_e}) \rangle, \end{aligned} \quad (11)$$

and the density is given by

$$\begin{aligned} n(\mathbf{r}) &= \sum_{\{i\}, \{j\}} d_i^* d_j \sum_{k, l, s} \psi_{k, s}^\dagger(\mathbf{r}) \psi_{l, s}(\mathbf{r}) \\ &\langle (i_1, s'_1), \dots, (i_{N_e}, s'_{N_e}) | c_{k, s}^\dagger c_{l, s} | (j_1, s_1), \dots, (j_{N_e}, s_{N_e}) \rangle. \end{aligned} \quad (12)$$

The wave function of $\psi_{k, s}(\mathbf{r}) = \psi_{k_x, k_y, s}(\mathbf{r})$ is a spinor, which can be written explicitly for different spins, $\psi_{k_x, k_y, +}(\mathbf{r}) = \begin{pmatrix} \psi_{k_x, k_y}(\mathbf{r}) \\ 0 \end{pmatrix}$ and $\psi_{k_x, k_y, -}(\mathbf{r}) = \begin{pmatrix} 0 \\ \psi_{k_x, k_y}(\mathbf{r}) \end{pmatrix}$.

In order to study the relation between the topological charge and the environment of the QD, we explicitly define the winding number

$$q = \frac{1}{2\pi} \oint d\phi = \frac{1}{2\pi} \oint \frac{\sigma_x(\mathbf{r}) d\sigma_y(\mathbf{r}) - \sigma_y(\mathbf{r}) d\sigma_x(\mathbf{r})}{\sigma_x(\mathbf{r})^2 + \sigma_y(\mathbf{r})^2}, \quad (13)$$

where $\phi(\mathbf{r}) = \arctan[\sigma_y(\mathbf{r})/\sigma_x(\mathbf{r})]$. The route of the integral is a closed path around a singularity of the ϕ field, then we can find the winding number of this particular vortex. However, in many-particle cases, there may be more than one vortices in the QD. So it is also worthy defining the overall winding number (OWN) of which the path is chosen around the edge and encloses all the possible vortices corresponding more than one singularity points of the ϕ field. The winding number is directly related to the topological feature of the in-plane spin field, and is therefore defined as the topological charge of the system.

III. TOPOLOGICAL FEATURES RELATED TO THE SIGN OF THE LANDÉ g FACTOR

In this work, we mainly focus on how the Coulomb interaction effects the topology of the system. But before that we should determine some features in the single-particle case, especially the topic how the topological charge is varied by the magnetic field. Then the many-body effect will be clear by comparing the two cases.

We study the generic case of an anisotropic QD in a magnetic field perturbatively. The unperturbed ground state of \mathcal{H}_0 is determined by the sign of the Landé g factor if $B > 0$, $\psi_-^{(0)} = (\psi_{0,0} \ 0)^T$ for $g < 0$ or $\psi_+^{(0)} = (0 \ \psi_{0,0})^T$ for $g > 0$. The perturbation is then \mathcal{H}_{L_z} plus the SOCs. The wavefunctions with the first-order corrections are

$$\begin{aligned} \psi_+^{(1)} &= \begin{pmatrix} \psi_{0,0} + iW\psi_{1,1}/2 \\ (\Gamma_{1,x} + i\Gamma_{2,x})\psi_{1,0} + (\Gamma_{2,y}^* + i\Gamma_{1,y}^*)\psi_{0,1} \end{pmatrix}, \\ \psi_-^{(1)} &= \begin{pmatrix} (\Gamma_{1,x} - i\Gamma_{2,x})\psi_{1,0} + (\Gamma_{2,y}^* - i\Gamma_{1,y}^*)\psi_{0,1} \\ \psi_{0,0} + iW\psi_{1,1}/2 \end{pmatrix}, \end{aligned} \quad (14)$$

where

$$\Gamma_{1,(x,y)} = \frac{1}{\sqrt{2}(|\Delta| + \hbar\Omega_{x,y})} \begin{pmatrix} -g_1 \frac{eB}{2} \ell_{x,y} + g_2 i \frac{\hbar}{\ell_{x,y}} \end{pmatrix}, \quad (16)$$

$$\Gamma_{2,(x,y)} = \frac{1}{\sqrt{2}(|\Delta| + \hbar\Omega_{x,y})} \begin{pmatrix} -g_2 \frac{eB}{2} \ell_{x,y} + g_1 i \frac{\hbar}{\ell_{x,y}} \end{pmatrix}. \quad (17)$$

$$W = \frac{\hbar\omega_c}{2\sqrt{\Omega_x\Omega_y}} \frac{\Omega_y - \Omega_x}{-\hbar(\Omega_x + \Omega_y)}, \quad (18)$$

where W is the anisotropic parameter and describes the anisotropy of the dot. Note that the wavefunctions are not normalized, but the normalization does not change the winding number. The in-plane spin fields can be calculated by Eq. (11),

$$\begin{aligned} \sigma_x^\pm(\mathbf{r}) &= \left[G_{1,x}^\pm \frac{x}{\ell_x} + G_{2,y}^\pm \frac{y}{\ell_y} \mp \left(G_{2,x}^\pm \frac{x}{\ell_x} + G_{1,y}^\pm \frac{y}{\ell_y} \right) W \frac{xy}{\ell_x \ell_y} \right] \\ &\times \psi_{0,0}(\mathbf{r}), \end{aligned} \quad (19)$$

$$\begin{aligned} \sigma_y^\pm(\mathbf{r}) &= \left[G_{2,x}^\pm \frac{x}{\ell_x} + G_{1,y}^\pm \frac{y}{\ell_y} \pm \left(G_{2,x}^\pm \frac{x}{\ell_x} + G_{1,y}^\pm \frac{y}{\ell_y} \right) W \frac{xy}{\ell_x \ell_y} \right] \\ &\times \psi_{0,0}(\mathbf{r}), \end{aligned} \quad (20)$$

where

$$G_{1,(x,y)}^\pm = \frac{(\pm 2\hbar - eB\ell_{x,y}^2) g_1}{2(|\Delta| + \hbar\Omega_{x,y})\ell_{x,y}}, \quad (21)$$

$$G_{2,(x,y)}^\pm = \frac{(\mp 2\hbar - eB\ell_{x,y}^2) g_2}{2(|\Delta| + \hbar\Omega_{x,y})\ell_{x,y}}. \quad (22)$$

Note that $\ell_{x,y}^2 = \hbar/(m^*\Omega_{x,y}) < 2\hbar/(m^*\omega_c)$ and $eB\ell_{x,y}^2 < 2\hbar$, then we have $\text{sign}\left[G_{1,(x,y)}^\pm\right] = \pm\text{sign}(g_1)$ and $\text{sign}\left[G_{2,(x,y)}^\pm\right] = \mp\text{sign}(g_2)$.

Specifically, if only the Rashba SOC is present, then (see the appendix)

$$q = \frac{G_{1,x}^\pm G_{1,y}^\pm}{\sqrt{(G_{1,y}^\pm G_{1,x}^\pm)^2}}. \quad (23)$$

Hence, $q = 1$ whatever the sign of g_1 is, which means that the sign of Rashba SOC, or say the direction of the external electric field, does not change the topological charge. In the same manner, if only the Dresselhaus SOC is present, then $q = -1$. Note that the calculation is based on an anisotropic dot and the result is not related to the anisotropic coefficient W . Therefore, the topological charge is analytically proven to be robust against the ellipticity of the dot, which has been studied only numerically in Ref.¹².

If both SOC's are present, the integral above becomes more complex. We are still able to obtain that (see the appendix)

$$q = \text{sgn}(G_{1,x}^\pm G_{1,y}^\pm - G_{2,x}^\pm G_{2,y}^\pm). \quad (24)$$

Consequently, we conclude that the topological charge is still $q = \pm 1$ when $G_{1,x}^\pm G_{1,y}^\pm > G_{2,x}^\pm G_{2,y}^\pm$ or $G_{1,x}^\pm G_{1,y}^\pm < G_{2,x}^\pm G_{2,y}^\pm$, respectively. Note that the sign of the topological charge is not only related to the either the strength or the sign of the SOC $g_{1,2}$. Only when the magnetic field is weak, the strength of the SOC can determine the topological charge. But, surprisingly, it is primarily determined by the sign of the Landé factor in a strong magnetic field.

If we consider a strong magnetic field $B \rightarrow \infty$, then $eB\ell_{x,y}^2 \rightarrow 2\hbar$, so that $G_{1,(x,y)}^+ \rightarrow 0, G_{2,(x,y)}^- \rightarrow 0$ and $G_{1,(x,y)}^- < 0, G_{2,(x,y)}^+ < 0$. If $g > 0$, then $q \rightarrow \text{sgn}(-G_{2,x}^+ G_{2,y}^+) = -1$, while $q \rightarrow \text{sgn}(G_{1,x}^- G_{1,y}^-) = 1$ if $g < 0$. Hence, we obtain that

$$q = -\text{sgn}(g). \quad (25)$$

It is safe to consider such a limitation $B \rightarrow \infty$ in the perturbation calculations. The energy scale of the unperturbative Hamiltonian \mathcal{H}_0 is $E_0 = \hbar\Omega_x/2 + \hbar\Omega_y/2$. The energy scale of \mathcal{H}_{L_z} is $E_{L_z} = \hbar\omega_c/2$, and the energy scale of \mathcal{H}_{SOC} is in the same order of $E_{SOC} = \hbar g_{1,2}/\ell_{x,y} + g_{1,2}eB\ell_{x,y}/2$. We can then compare these energy scales in the limit of $B \rightarrow \infty$. It is obvious that $E_{L_z} < E_0$ always, since $\frac{1}{2}\omega_c < \Omega_{x,y} = \sqrt{\omega_c^2/4 + \omega_{x,y}^2}$. Moreover, $E_{SOC} = g_{1,2}\sqrt{\hbar m^*\Omega_{x,y}}\left(1 + \frac{1}{2}\frac{\omega_c}{\Omega_{x,y}}\right) < 2g_{1,2}\sqrt{\hbar m^*\Omega_{x,y}}$, and then $E_{SOC}/E_0 \rightarrow 0$ when the magnetic field is very large ($\Omega_{x,y} \rightarrow \infty$).

On the other hand, in the perturbative states in Eqs. (14) and (15), the corrections of the unperturbative states are Γ and W shown in Eqs. (16-18). When

$B \rightarrow \infty$, the anisotropic parameter is always $W < 1$, and the perturbation of the SOC's \mathcal{H}_{SOC} provides the corrections in Eqs. (16) and (17) also approach zero, $\Gamma_{(1,2),(x,y)} \propto 1/\sqrt{\Omega_{x,y}} \rightarrow 0$. Indeed, when $B \rightarrow \infty$, the in-plane spin fields vanish and the spin textures disappear. However, we can suppose a very large magnetic field where the perturbation theory is valid and the spin textures are still available.

The sign of the Landé factor (a difficult problem experimentally⁴⁴) may therefore be obtained by detecting the topological charge. This important property in Eq. (25) is not only valid in the single-electron case, but also works in the two-electron case. We shall confirm this point below in the numerical calculations.

The Landé factors of the two systems, InAs dot and ZnO dot, have opposite signs. The unique properties of the later system⁴⁵ have been explored only recently⁴⁶⁻⁵⁰. By comparing the InAs quantum dots, and the ZnO dots, we could determine how the Landé factor influences the topological spin textures and the density profiles of the electrons. For the InAs dot, the effective mass of electron is $m_{\text{InAs}}^* = 0.042m_e$, Landé factor $g_{\text{InAs}} = -14$ and the dielectric constant $\epsilon_{\text{InAs}} = 14.6$. For a ZnO dot, the effective mass is $m_{\text{ZnO}}^* = 0.24m_e$, Landé factor $g_{\text{ZnO}} = 4.3$ and dielectric constant $\epsilon_{\text{ZnO}} = 8.5$.

In these single-electron systems, we consider the case when both SOC's are present. The numerical results are shown in Fig. 1: with increase of the magnetic field, we clearly see how the spin textures evolve. In the InAs dot, if $g_1 > g_2$, the topological charge is always $q = 1$. If $g_1 < g_2$, the topological charge is $q = -1$ in a weak magnetic field $B < 6.5\text{T}$, but $q = 1$ in a strong magnetic field due to the fact that $g_{\text{InAs}} < 0$ [Figs. 1(a) and 1(c)]. In a ZnO dot, if $g_1 < g_2$, we have $q = -1$. But if $g_1 > g_2$, the topological charge is $q = 1$ in a weak magnetic field $B < 4.5\text{T}$, while it changes to $q = -1$ in a strong magnetic field since $g_{\text{ZnO}} > 0$ [Figs. 1(b) and 1(d)]. The important finding in Eq. (25) perfectly agrees with our numerical studies [Fig. 1]. We note that the spin textures are topological trivial $q = 0$, when $G_{1,x}^\pm G_{1,y}^\pm = G_{2,x}^\pm G_{2,y}^\pm$.

IV. QUANTUM DOT HELIUM

If there is more than one electron confined in the dot, we must consider the Coulomb interaction. Indeed, the Coulomb interaction is not negligible and provides the various magnetic signatures in the system. We would like to determine how the Coulomb interaction affects the topological properties of the many-electron dots. Therefore, we exactly diagonalize $\mathcal{H}_T = \mathcal{H} + \mathcal{H}_C$ to obtain the electron density, the spin textures, $\langle L_z \rangle$, as well as the winding number. The spin textures depend on the density profile, and conversely, the density profile can be modified by the spin textures. The density profile of the ground state is closely related to $\langle L_z \rangle$. We study the relations among those quantities in this section. For simplicity and without loss of generality, we consider only

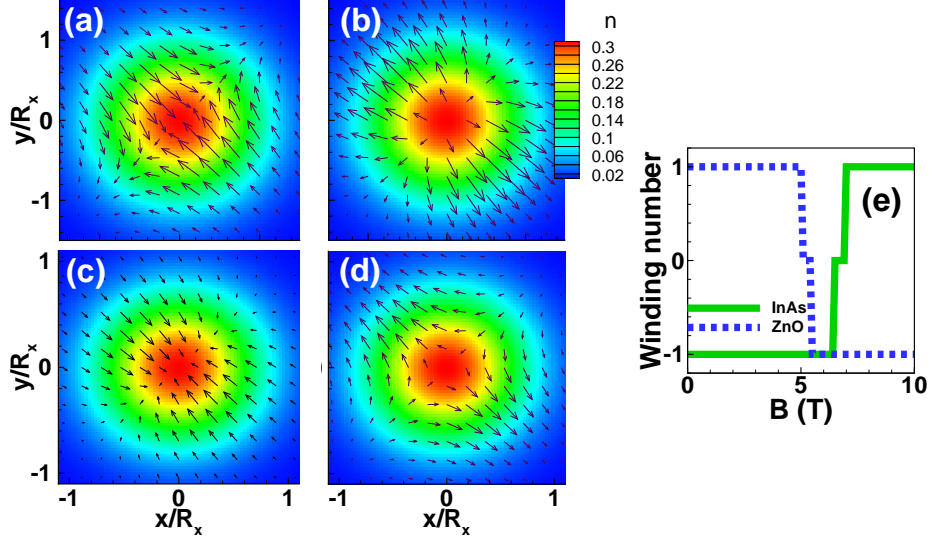


FIG. 1: (Colors online) The evolution of spin textures in dots with magnetic fields. Hereafter, the colors of the two-dimensional pictures represent the density of the electron, which is defined by Eq. (12), and the arrows represent the in-plane spin field $(\sigma_x(\mathbf{r}), \sigma_y(\mathbf{r}))$. The magnetic fields are (a) $B = 0.1\text{T}$, and (c) $B = 10\text{T}$ for an InAs dot, and (b) $B = 0.1\text{T}$, (d) $B = 10\text{T}$ for a ZnO dot. We consider $R_x = 15\text{ nm}$, $R_y = 14\text{ nm}$. The SOC's are $\hbar g_1 = \hbar g_2/2 = 10\text{ meV}\cdot\text{nm}$ for the InAs dot, and $\hbar g_1 = 2\hbar g_2 = 5\text{ meV}\cdot\text{nm}$ for the ZnO dot. (e) The winding numbers of the two cases.

the two-electron case, viz. the quantum dot helium.

In our exact diagonalization scheme, we keep the quantum number of the harmonic oscillator $n_x, n_y \in [0, 5]$, and so that 72 single-electron states are taken into account. This cut-off is sufficient for the energy convergence.

A. Two-electron states in isotropic dots with one type of SOC

We consider the isotropic QD in this subsection. In such a QD without the SOC's, $\langle L_z \rangle$ is quantized with the increase of the magnetic field. $\langle L_z \rangle$ is always an integer and the system has the rotational symmetry.

With either one of the SOC's (Rashba or Dresselhaus), $\langle L_z \rangle$ is not a good quantum number, and $\langle L_z \rangle$ is no longer an integer, as shown in Figs. 2(a) and 2(b). The spin texture is a single vortex with the topological charge $q = \pm 1$ in a magnetic field for a Rashba dot or a Dresselhaus dot, respectively. The density profile is still rotationally invariant. The rotation matrices for the Rashba SOC (U_R) and the Dresselhaus SOC (U_D) are¹²

$$U_R(\theta) = \begin{pmatrix} \cos \theta & \sin \theta \\ -\sin \theta & \cos \theta \end{pmatrix}, \quad U_D(\theta) = U_R(-\theta), \quad (26)$$

where θ is the angle in the polar coordinate of the $x - y$ plane, are still valid to protect the rotational symmetry of the system as well as the density of electrons if there is only one SOC present. We show the $\langle L_z \rangle$ in terms of the magnetic field in an InAs QD and in a ZnO dot with Rashba SOC in Fig. 2(a) and Fig. 2(b), respectively. The

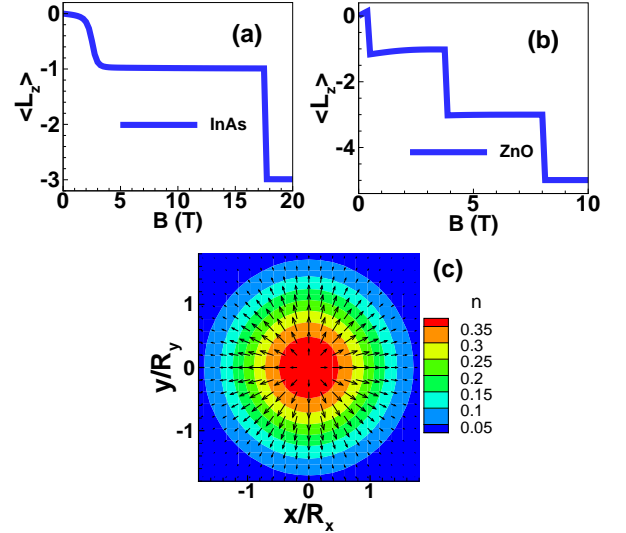


FIG. 2: (Colors online) $\langle L_z \rangle$ of the two-electron states in (a) an InAs dot and (b) in a ZnO dot with the Rashba SOC. The size of the two dots is the same, $R_x = R_y = 15\text{ nm}$. The strengths of the SOC are $\hbar g_1 = \hbar g_2 = 20\text{ meV}\cdot\text{nm}$ for the InAs dot, and $\hbar g_1 = \hbar g_2 = 5\text{ meV}\cdot\text{nm}$ for the ZnO dot. (c) The density and the spin texture of the two-electron InAs dot at $B = 2.5\text{T}$, where $\langle L_z \rangle = -0.4867$.

density profile and spin texture of the InAs dot are shown when $B = 2.5\text{T}$ and $\langle L_z \rangle = -0.4867$ in Fig. 2(c).

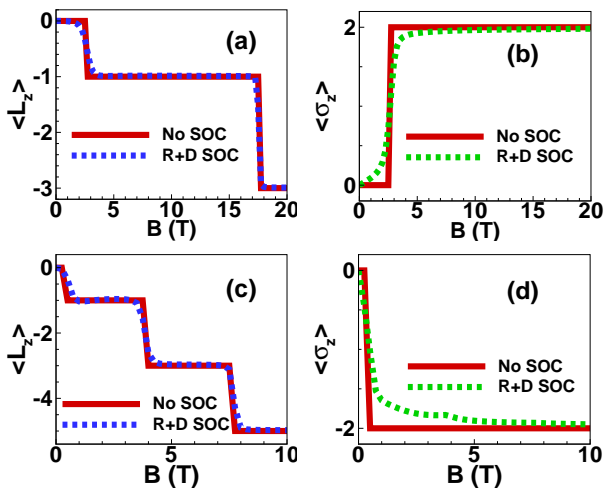


FIG. 3: (Colors online) (a) $\langle L_z \rangle$ and (b) $\langle \sigma_z \rangle$ of the two-electron state in an InAs dot with and without the SOCs. The strengths of the SOCs are $\hbar g_1 = \hbar g_2 = 20$ meV·nm. (c) $\langle L_z \rangle$ and (d) $\langle \sigma_z \rangle$ of the two-electron state in a ZnO dot with and without the SOCs. The strengths of the SOCs are $\hbar g_1 = \hbar g_2 = 5$ meV·nm. The size of the two dots is the same, $R_x = R_y = 15$ nm.

B. Two-electron states in isotropic InAs dots with both two SOCs

$\langle L_z \rangle$ displays a smooth transition with the magnetic field when both the SOCs are present. Then the effective rotational symmetry of the density can be broken, since the spin field no longer has the rotational symmetry. It is therefore more interesting to discuss in detail how the two SOCs and the Coulomb interaction jointly influence the spin textures and then the density profiles with increasing magnetic field. For simplicity, we consider the case $g_1 = g_2$ in an isotropic dot only [Fig. 3]. The discontinuous transitions in $\langle L_z \rangle$ are smoothed out in the presence of the SOCs as well. Strictly speaking, there is no integer plateau of $\langle L_z \rangle$. However, we can still mark the plateaus where the system shows $\langle L_z \rangle$ very close to being integers. We also show $\langle \sigma_z \rangle$ in Fig. 3, since it is measurable in an NMR experiment⁵¹.

In the InAs dot without the SOC, no spin textures appear and the density profile evolves from a dot to a ring as the magnetic field increases, since $\langle L_z \rangle$ jumps from 0 to -3 when the magnetic field increases up to 20T. Due to the existence of the confinement, the degeneracy of the Landau level is lifted, and the Coulomb interaction mixes single-electron levels with different angular momentum to quantize $\langle L_z \rangle$. When the SOCs are present, spin textures appear to deform the density profile, especially when $\langle L_z \rangle$ is in the region between two plateaus.

Since the spin textures are much richer in quantum-dot helium than those in a single-electron dot (QD hydrogen), we need to use the concept of the overall winding number (OWN) which is equivalent to the total topo-

logical charge. It can also be obtained by summing the topological charge for each vortex in the system.

We consider here the dot with $R_x = R_y = 15$ nm, and SOCs $\hbar g_1 = \hbar g_2 = 20$ nm·meV. With an increase of the magnetic field, the density profile and spin textures evolve as follows (or see the rainbow bar in Fig. 4):

(i) $B = 0$ T, the spin textures are cancelled by the time reversal symmetry; (ii) $0 < B < 2$ T, the density profile and spin textures are close to the single-particle case shown in Fig. 4(a). $\langle L_z \rangle$ is in the first plateau $\langle L_z \rangle \approx 0$; (iii) $2 < B < 4.5$ T, the spin textures are shown in Fig. 4(b). There are three vortices located along the line $x = -y$, in which one with $q = 1$ locates at the center and the other two with topological charge $q = -1$ locate at $(-0.4, 0.4)$ and $(0.4, -0.4)$. The OWN is thus obtained by summing all the three charges, $q = -1$. The density is an elliptic dot stretched along $x = -y$, since $\langle L_z \rangle$ is between the two plateaus; (iv) $4.5 < B < 15$ T, the spin textures are shown in Fig. 4(c), there are still three vortices: two have topological charge $q = 1$ [locate at $(0.5, 0.5)$ and $(-0.5, -0.5)$] and the other has $q = -1$ at the origin, but in the line of $x = y$. The OWN is changed to $+1$. The density is again close to that of an isotropic dot, since $\langle L_z \rangle$ is located on the plateau; (v) $15 < B < 17.3$ T, the three vortices merge toward the center, while the density is again stretched but along the line $x = -y$, which is shown in Fig. 4(d); (vi) Magnetic field around 17.5T, where $\langle L_z \rangle$ is between two plateaus -1 and -3 , the density is split into two dots [Fig. 4(e)], i.e., significantly different from all the other cases. Two vortices with $q = 1$ locate at the two density dots, and one with $q = -1$ at origin. The OWN is thus 1; (vii) $17.7 < B < 20$ T, the split rings of density is shown in Fig. 4(f); (viii) $B > 20$ T, the density is not split by the SOCs [Fig. 4(g)], since $\langle L_z \rangle \approx -3$ is again back to the plateau, and the OWN is still 1.

C. Two-electron states in isotropic ZnO dots with both two SOCs

We now consider the ZnO dot where the Coulomb interaction is much stronger than that for the InAs dot⁴⁹. Without the SOC, the density has a ring-shape even at $\langle L_z \rangle = 0$. With the SOCs we are able to study how important the role of Coulomb interaction is in splitting the density. Note that the SOCs in ZnO is much weaker, so we consider $\hbar g_1 = \hbar g_2 = 5$ meV·nm.

Just as in the case of the InAs dot, we find the following spin-density textures with increase of the magnetic field up to 10T (or see the rainbow bar in Fig. 4):

(i) $B = 0$, the spin textures are cancelled by the time reversal symmetry; (ii) $0 < B < 0.2$ T, the spin textures and the density are close to that of the single-particle case [Fig. 5(a)]; (iii) $0.2 < B < 1.9$ T [Fig. 5(b)]: $\langle L_z \rangle$ is between the two plateaus $\langle L_z \rangle \approx 0$ and $\langle L_z \rangle \approx -1$. So the density splits and meanwhile the spin textures split, two vortices with $q = 1$ at $(-0.8, 0.8)$ and $(0.8, -$

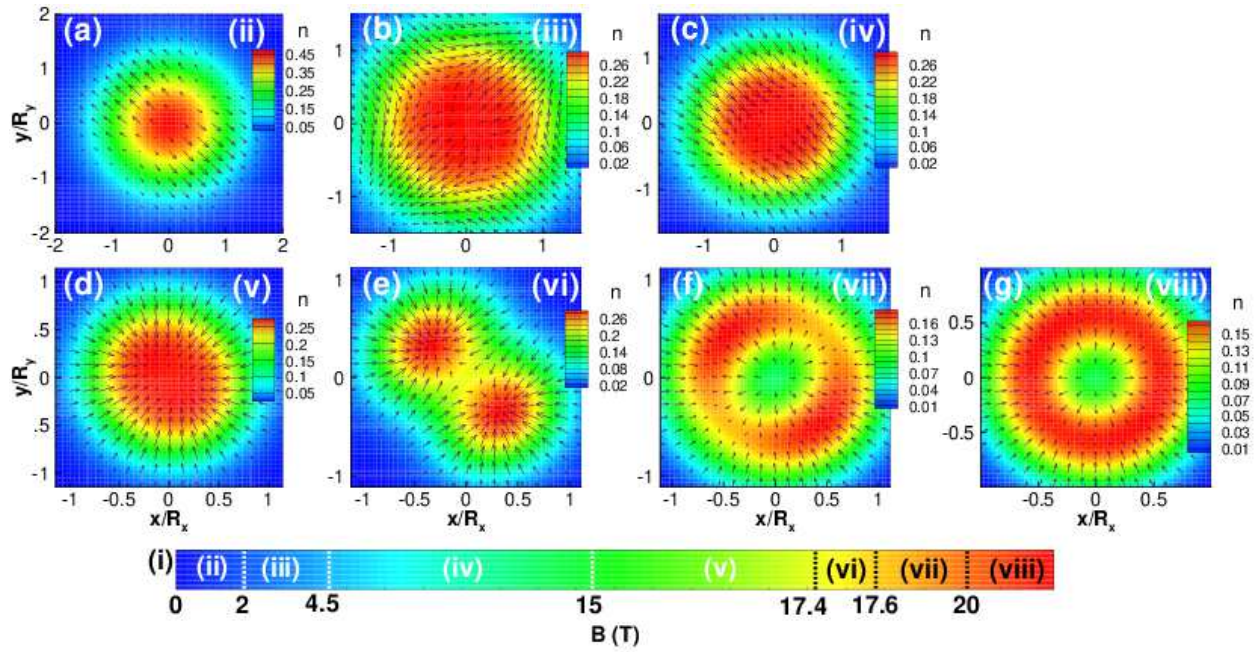


FIG. 4: (Color online) The density profiles of a two-electron InAs dot, $R_x = R_y = 15$ nm, with SOCs $\hbar g_1 = \hbar g_2 = 20$ nm·meV. The colors stands for the density n of the two electrons. The magnetic fields are (a) 1T; (b) 3.7T; (c) 6T; (d) 12T; (e) 17.5T; (f) 18T; (g) 23T. The Roman numerals are corresponding to the states described in the text.

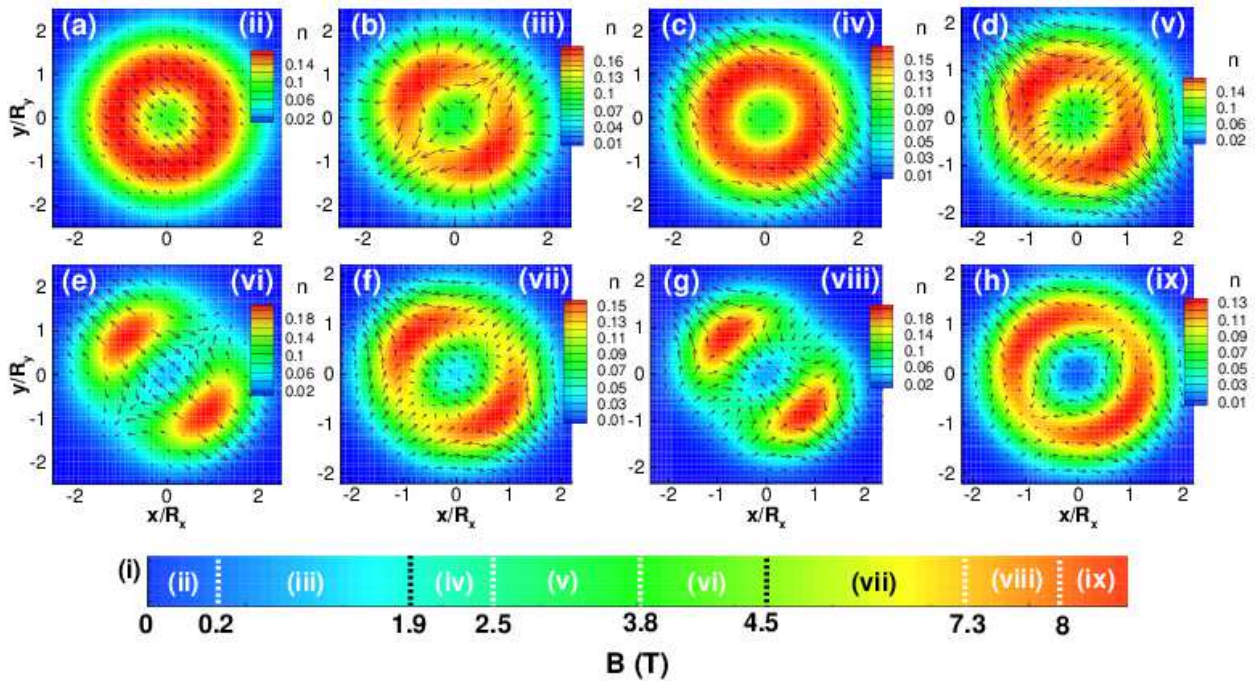


FIG. 5: (Color online) The density profiles of a two-electron dot, $R_x = R_y = 15$ nm, with SOCs $\hbar g_1 = \hbar g_2 = 5$ nm·meV. The magnetic fields are (a) 0.1T; (b) 0.7T; (c) 2.2T; (d) 3T; (e) 4T; (f) 7T; (g) 7.5T; (h) 9T.

0.8) and one vortex with $q = -1$ at origin. The OWN is then 1; (iv) $1.9 < B < 2.5\text{T}$ [Fig. 5(c)], the OWN changes to $q = -\text{sgn}(g_{\text{zno}}) = -1$. The reason is the same as for the InAs dot – the single-electron treatment; (v) $2.5 < B < 3.8\text{T}$ [Fig. 5(d)], the density starts to split between the two plateaus $\langle L_z \rangle \approx -1$ and $\langle L_z \rangle \approx -3$. The density profile is similar to the case (iii) but the topological features are inverted, two vortices with $q = -1$ at $(-0.6, 0.6)$ and $(0.6, -0.6)$ while one vortex with $q = 1$ at origin. The OWN is -1 ; (vi) $3.8 < B < 4.5\text{T}$ [Fig. 5(e)], the density profile has a two-dot shape. The spin textures are not very regular, but we can find that two vortices at the two dots are with topological charge 1 and the third one is $q = -1$ at origin; (vii) $4.5 < B < 7.3\text{T}$ [Fig. 5(f)], the density merges to a split ring, when $\langle L_z \rangle$ enters to a plateau. The spin textures are even more complex, three vortices with $q = -1$ at $(-0.8, 0.8)$, $(0, 0)$, and $(0.8, -0.8)$ and two vortices with $q = 1$ at $(0.5, 0.5)$ and $(-0.5, -0.5)$, so the OWN is $q = -1$; (viii) $7.3 < B < 8\text{T}$ [Fig. 5(g)], the density splits to two dots again between the two plateau between the two plateaus $\langle L_z \rangle \approx -3$ and $\langle L_z \rangle \approx -5$. The two vortices with $q = -1$ are associated with the two density dots and one vortex with $q = 1$ at origin; (ix) $B > 8\text{T}$ [Fig. 5(f)], the density merges to a split ring, again. The OWN is -1 , however, the details of the vortices in the ring are not very clear in the figure.

D. Summary of the density evolution in the isotropic QD helium with both SOC's included

Overall, the density profile evolves with the change of $\langle L_z \rangle$. Generally for the density profile, whatever the material is, the dot-shape is stretched and the ring-shape splits by the SOC's when $\langle L_z \rangle$ is far away from an integer, while it merges when $\langle L_z \rangle$ enters a plateau near an integer. The evolution of the density profile with increase of magnetic field falls to a split-merge cycle.

E. Coulomb interaction effects

The deformation of the density profile can be understood as following. When $\langle L_z \rangle$ is in the plateau, the many-body state is basically composed by the eigen states of L_z , $|\Psi\rangle \approx |n_1, l_1, s_1\rangle |n_2, l_2, s_2\rangle$, where l_1, l_2 are the quantum number of L_z and $l_1 + l_2 = \langle L_z \rangle$, n_1, n_2 are Landau level indices and s_1, s_2 are the spin indices of the system. The density has the rotational symmetry since $\langle L_z \rangle$ is still an integer and L_z commutes with rotation with respect to the z axis. The SOC's accompanied by the Coulomb interaction make the $\langle L_z \rangle$ deviate from the plateaus. Then the wave function may not be so much related to two eigenstates of L_z with the same phase (the wave function is given by the superposition of many eigenstates of L_z with complex phases). Moreover, both of the two SOC's exist and neither U_R nor U_D protects the rotational symmetry, since $L_z \pm \sigma_z/2$ does

not commute with the SOC's any more. So the rotational symmetry of the wave function and the density can be broken. On the other hand, the density deformation induces the changes of the Coulomb interaction. When all these conditions combine together, the density splitting occurs only when $\langle L_z \rangle$ is far away from the integer plateau. If there is no Coulomb interaction, then no mixing among single-electron levels appears, so that $\langle L_z \rangle \rightarrow \sim -1$ and no more transition happens, then the split-merge cycle of the density deformation disappears. The non-interacting picture is apparently incorrect in the many-particle cases.

We note that the topological features are tunable by adding electron in the system. We consider an InAs dot with $\hbar g_1 = \hbar g_2 = 20\text{meV} \cdot \text{nm}$. The sign of the OWN is altered in the QD helium by the many-body effect as shown in Fig. 6(a). It is very interesting that the OWN is even related to $\langle L_z \rangle$. The windows of inverse of the OWNs for the QD helium (comparing with the cases of QD hydrogen) are open when $\langle L_z \rangle$ is converted from 0 to -1 and $\langle \sigma_z \rangle$ is converted from 0 to 2. When $B < 2.8\text{T}$, the topological inversion is also related to the region $0 < \langle \sigma_z \rangle < 1$ shown in Fig. 6(d), which provides the clue of the indirect measurement of the topological charge.

In order to determine how the Coulomb interaction affects the topological properties of the system, we compare the interacting two-electron state and the non-interacting two-electron state. We consider the fixed $\hbar g_2 = 20\text{meV} \cdot \text{nm}$ and varied g_1 in the InAs dot. The OWNs, $\langle L_z \rangle$, and $\langle \sigma_z \rangle$ of the two interacting electrons states are indicated in Figs. 6(b), 6(c), and 6(d), respectively. The region of the inverse of the topological charge, comparing with the single electron state is basically covered by the region of the transition $\langle L_z \rangle = 0 \rightarrow -1$. As discussed above, the SOC's associated with the Coulomb interaction change the wave function mostly in this region between two plateaus of $\langle L_z \rangle$. Hence, it is mostly possible to change the topological features in such regions. The OWNs, $\langle L_z \rangle$, and $\langle \sigma_z \rangle$ of the two non-interacting electrons are shown in Figs. 6(g), 6(h), and 6(i), respectively. The Coulomb interaction significantly shifts and compresses the regions of all of these quantities (OWNs, $\langle L_z \rangle$, and $\langle \sigma_z \rangle$).

We further note that when the magnetic field is strong, the OWN should then be given by the single-particle case. The contour of calculating the OWN is far away from the center of the quantum dot, where the density of electrons is small and the Coulomb interaction plays a less important role. The SOC's determine the topological feature of the system, i.e. $q \rightarrow -\text{sgn}(g)$.

F. Two-electron states in anisotropic dots

We also study the more practical case: how the ellipticity affects the spin-density profiles. Firstly, we consider a slightly strained dot, $R_x = 15\text{ nm}$ and $R_y = 14.9\text{ nm}$. All the states in Figs. 4 and 5 are unaltered. However, the

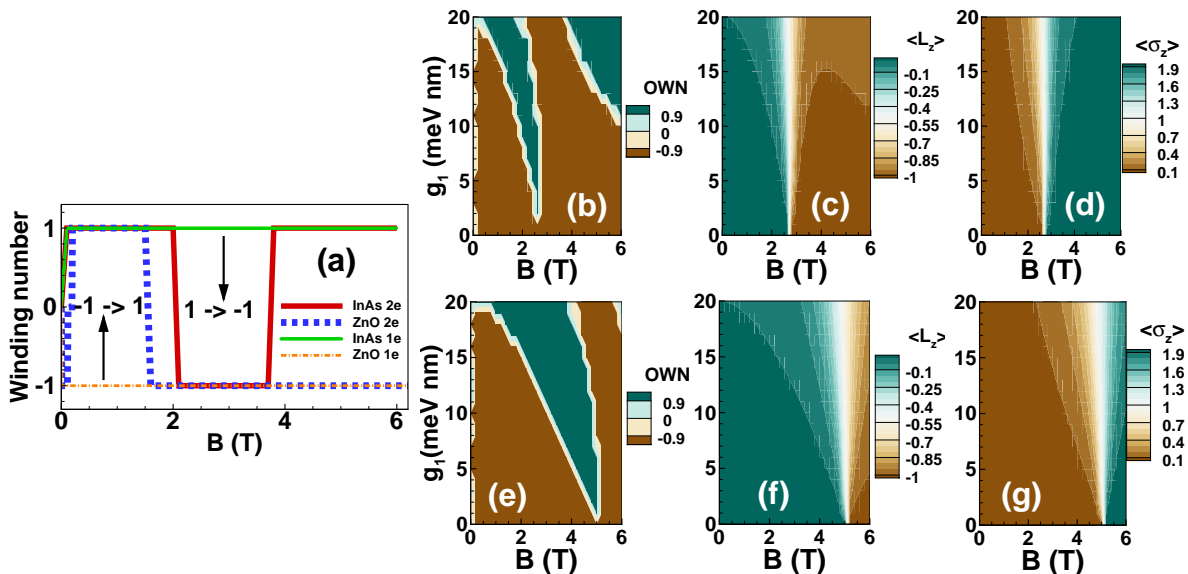


FIG. 6: (Color online) (a) The OWN of the QD helium where $R_x = R_y = 15$ nm, $\hbar g_1 = \hbar g_2 = 20$ nm \cdot meV for the InAs dot, and $R_x = R_y = 15$ nm, $\hbar g_1 = \hbar g_2 = 5$ nm \cdot meV for the ZnO dot. For comparison the OWNs of the QD hydrogen with $g_1 = g_2$ are also shown. The arrows show the OWN reversed by the Coulomb interaction. (b) The OWN, (c) $\langle L_z \rangle$, and (d) $\langle \sigma_z \rangle$ for the InAs QD helium with tunable $\hbar g_1 \in [0, 20]$ meV \cdot nm and fixed $\hbar g_2 = 20$ meV \cdot nm. In comparison, (e) the OWN, (f) $\langle L_z \rangle$, and (g) $\langle \sigma_z \rangle$ of the ground state of the two non-interacting electrons are also plotted.

spin textures are slightly twisted and the density profile is rotated anticlockwise toward the $-x$ axis.

In Fig 7, the dot is strained seriously and without the SOC, e.g. $R_x = 15$ nm, $R_y = 10$ nm. The density profile split into two dots along the long-axis when $B > 4$ T, where the plateau of $\langle L_z \rangle$ disappears and $\langle L_z \rangle$ is far away from an integer. The spin textures with only one SOC were reported earlier in¹², the density can not be rotated. With both the SOCs, the spin textures rotate the density clockwise slightly, $< 5^\circ$.

V. CONCLUSION

In summary, we have shown that the winding number (topological charge) uniquely depends on the sign of Landé g factor of the material in a strong magnetic field, and in the presence of both Rashba and dresselhaus SOCs. We also analytically demonstrate that this number is robust against the ellipticity of the dot. With both the SOCs present, the spin textures can deform the density profile of the quantum-dot helium, since the transition of $\langle L_z \rangle$ is smoothed. Between two plateaus of $\langle L_z \rangle$, the rotational symmetry is broken. In such regions, the dot-shaped density becomes stretched, while a ring-shaped density is split, with the coupling of SOCs. The topological features at the edge where the contour of

calculating the OWN is far away from the center follows the rule of the QD hydrogen, $q = -\text{sgn}(\Delta)$ when the magnetic field is sufficiently strong.

The Coulomb interaction accompanied with both the SOCs can reverse the sign of the total topological charge around the region of the magnetic field where $\langle L_z \rangle : 0 \rightarrow -1$. A stronger Coulomb interaction can make this topological transition happen in a weaker magnetic field. Note that we consider only two electrons in the system, more electrons and more complex Coulomb interaction may change the topology in a more significant way. It perhaps indicates that in other topological non-trivial systems, the Coulomb interaction may be also important and needs to be carefully treated.

The significance of these findings is that the topological charge of the electron state is easily tunable by the perpendicular magnetic field alone if both of the SOCs are intrinsic, which thus provides to control the topology of the system in spintronics and quantum information.

VI. ACKNOWLEDGEMENT

W.L. acknowledges support by the NSF-China under Grant No. 11804396. W.L. also thanks Jian Sun and Yu Zhou for helpful discussions. Computation time was provided by Calcul Québec and Compute Canada.

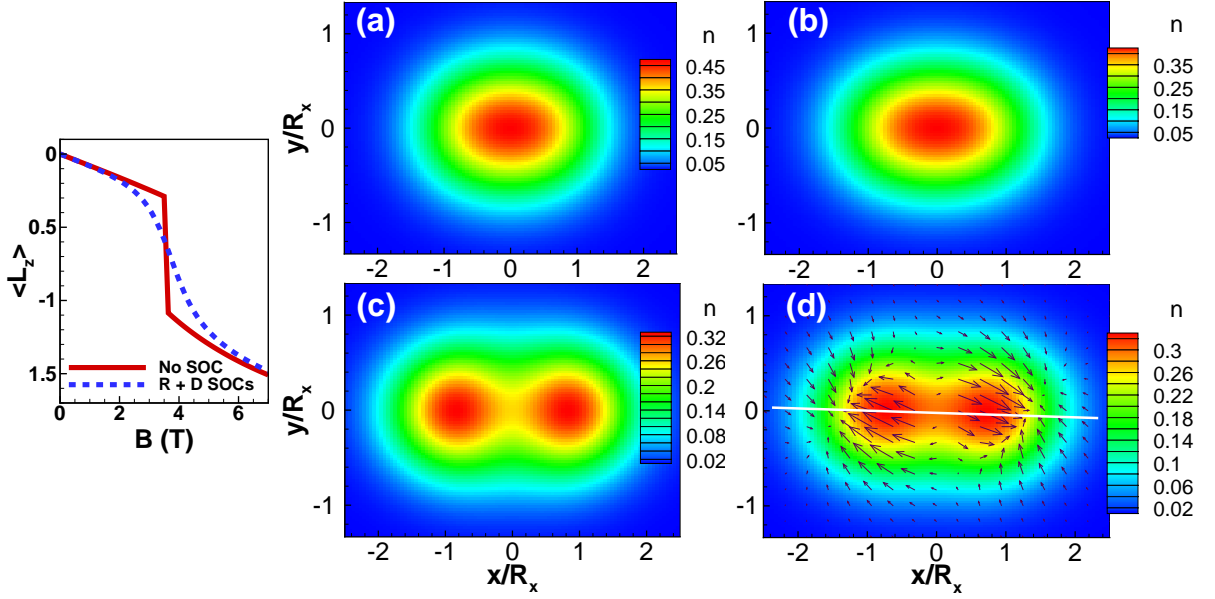


FIG. 7: (Color online) (a) $\langle L_z \rangle$ for the InAs quantum dot helium $R_x = 15$ nm, $R_y = 10$ nm, with and without SOCs. The SOCs are $g_1 = g_2 = 20$ nm \cdot meV. The density profiles of the quantum dot without SOC at (a) $B = 0$ T, (b) $B = 3$ T and (c) $B = 5$ T. (d) The SOCs are coupled to such a dot at $B = 5$ T. The white line is a guidance to eyes.

VII. APPENDIX

We derive the topological charge explicitly shown in Eqs. (23) and (24) here. We use the short note $G^\pm = G$ in Eqs. (19) and (20), and then the topological charge for a Rashba dot ($g_1 \neq 0, g_2 = 0$) is

$$\begin{aligned}
 q &= \frac{1}{2\pi} \oint \frac{\sigma_x^R d\sigma_y^R - \sigma_y^R d\sigma_x^R}{\sigma_x^2 + \sigma_y^2} \\
 &= \frac{1}{2\pi} \oint \left[(G_{1,x} \cos \theta + r^2 G_{1,y} W \cos \theta \sin^2 \theta) d(G_{1,y} \sin \theta - r^2 G_{1,x} W \cos^2 \theta \sin \theta) \right. \\
 &\quad \left. - (G_{1,y} \sin \theta - r^2 G_{1,x} W \cos^2 \theta \sin \theta) d(G_{1,x} \cos \theta + r^2 G_{1,y} W \cos \theta \sin^2 \theta) \right] \\
 &\quad / \left[(G_{1,x} \cos \theta + r^2 G_{1,y} W \cos \theta \sin^2 \theta)^2 + (G_{1,y} \sin \theta - r^2 G_{1,x} W \cos^2 \theta \sin \theta)^2 \right],
 \end{aligned}$$

where σ_i^R is the spin field with $g_2 = 0$ in Eqs. (19) and (20), and $r = \sqrt{x^2 + y^2}$. Then the topological charge is

$$q = \frac{1}{2\pi} \oint \frac{G_{1,x} G_{1,y} (1 + r^4 W^2 \cos^2 \theta \sin^2 \theta) - r^2 W (G_{1,x}^2 \cos^2 \theta + G_{1,y}^2 \sin^2 \theta) (\cos^2 \theta - \sin^2 \theta)}{(1 + r^4 W^2 \cos^2 \theta \sin^2 \theta) (G_{1,y}^2 \sin^2 \theta + G_{1,x}^2 \cos^2 \theta)},$$

The integral is obtained by considering a circular contour of which the center is at the origin and the radius is r ,

$$q = \frac{1}{2\pi} \int_0^{2\pi} d\theta \frac{G_{1,x} G_{1,y}}{G_{1,y}^2 \sin^2 \theta + G_{1,x}^2 \cos^2 \theta} - \frac{1}{2\pi} \int_0^{2\pi} d\theta \frac{r^2 W \cos(2\theta)}{(1 + r^4 W^2 \cos^2 \theta \sin^2 \theta)} = \frac{G_{1,x} G_{1,y}}{\sqrt{G_{1,y}^2} \sqrt{G_{1,x}^2}},$$

which is the same as Eq. (23). It is clear that the integral with W in the integrand vanishes, so the elliptical effect vanishes.

For the Dresselhaus dot ($g_1 = 0, g_2 \neq 0$), it is in the same way to obtain that $q = -1$. The charge is

$$\begin{aligned} q &= \frac{1}{2\pi} \oint \frac{\sigma_x^D d\sigma_y^D - \sigma_y^D d\sigma_x^D}{\sigma_x^2 + \sigma_y^2} \\ &= \frac{1}{2\pi} \oint [(G_{2,y} \sin \theta + r^2 G_{2,x} W \sin \theta \cos^2 \theta) d(G_{2,x} \cos \theta - r^2 G_{2,y} W \cos \theta \sin^2 \theta) \\ &\quad - (G_{2,x} \cos \theta - r^2 G_{2,y} W \cos \theta \sin^2 \theta) d(G_{2,y} \sin \theta + r^2 G_{2,x} W \sin \theta \cos^2 \theta)] \\ &\quad / \left[(G_{2,y} \sin \theta + r^2 G_{2,x} W \sin \theta \cos^2 \theta)^2 + (G_{2,x} \cos \theta - r^2 G_{2,y} W \cos \theta \sin^2 \theta)^2 \right], \end{aligned}$$

where σ_i^D is the spin field with $g_1 = 0$ in Eqs. (19) and (20). Then

$$\begin{aligned} q &= \frac{1}{2\pi} \oint \frac{-G_{2,y} G_{2,x} (1 + r^4 W^2 \cos^2 \theta \sin^2 \theta) - r^2 W (G_{2,x}^2 \cos^2 \theta + G_{1,y}^2 \sin^2 \theta) (\cos^2 \theta - \sin^2 \theta)}{(1 + r^4 W^2 \cos^2 \theta \sin^2 \theta) (G_{2,x}^2 \cos^2 \theta + G_{2,y}^2 \sin^2 \theta)} \\ &= -\frac{1}{2\pi} \int_0^{2\pi} d\theta \frac{G_{2,y} G_{2,x}}{G_{2,x}^2 \cos^2 \theta + G_{2,y}^2 \sin^2 \theta} - \frac{1}{2\pi} \int_0^{2\pi} d\theta \frac{r^2 W \cos(2\theta)}{(1 + r^4 W^2 \cos^2 \theta \sin^2 \theta)} = -\frac{G_{2,x} G_{2,y}}{\sqrt{G_{2,y}^2} \sqrt{G_{2,x}^2}}. \end{aligned}$$

The general case with both of the two SOCs reads,

$$q = \frac{1}{2\pi} \oint \frac{\sigma_x d\sigma_y - \sigma_y d\sigma_x}{\sigma_x^2 + \sigma_y^2} = \frac{1}{2\pi} \oint \frac{(\sigma_x^R + \sigma_x^D) d(\sigma_y^R + \sigma_y^D) - (\sigma_y^R + \sigma_y^D) d(\sigma_x^R + \sigma_x^D)}{(\sigma_x^R + \sigma_x^D)^2 + (\sigma_y^R + \sigma_y^D)^2}.$$

The denominator is

$$\begin{aligned} &(\sigma_x^R)^2 + (\sigma_y^R)^2 + (\sigma_x^D)^2 + (\sigma_y^D)^2 + 2\sigma_x^R \sigma_x^D + 2\sigma_y^R \sigma_y^D \\ &= (1 + r^4 W^2 \cos^2 \theta \sin^2 \theta) \left[(G_{1,x} \cos \theta + G_{2,y} \sin \theta)^2 + (G_{1,y} \sin \theta + G_{2,x} \cos \theta)^2 \right], \end{aligned}$$

where

$$2\sigma_x^R \sigma_x^D + 2\sigma_y^R \sigma_y^D = 2(G_{1,x} G_{2,y} + G_{1,y} G_{2,x}) \sin \theta \cos \theta (1 + r^4 W^2 \sin^2 \theta \cos^2 \theta).$$

The nominator is

$$\begin{aligned} &(\sigma_x^R + \sigma_x^D) d(\sigma_y^R + \sigma_y^D) - (\sigma_y^R + \sigma_y^D) d(\sigma_x^R + \sigma_x^D) \\ &= (\sigma_x^R d\sigma_y^R - \sigma_y^R d\sigma_x^R + \sigma_x^D d\sigma_y^D - \sigma_y^D d\sigma_x^D) + (\sigma_x^R d\sigma_y^D + \sigma_x^D d\sigma_y^R - \sigma_y^R d\sigma_x^D - \sigma_y^D d\sigma_x^R), \end{aligned}$$

and

$$\begin{aligned} \sigma_x^R d\sigma_y^D &= (G_{1,x} \cos \theta + r^2 G_{1,y} W \cos \theta \sin^2 \theta) (-G_{2,x} \sin \theta + r^2 G_{2,y} W \sin^3 \theta - 2r^2 G_{2,y} W \cos^2 \theta \sin \theta), \\ \sigma_x^D d\sigma_y^R &= (G_{2,y} \sin \theta + r^2 G_{2,x} W \sin \theta \cos^2 \theta) (G_{1,y} \cos \theta - r^2 G_{1,x} W \cos^3 \theta + 2r^2 G_{1,x} W \cos \theta \sin^2 \theta), \\ \sigma_y^R d\sigma_x^D &= (G_{1,y} \sin \theta - r^2 G_{1,x} W \cos^2 \theta \sin \theta) (G_{2,y} \cos \theta + r^2 G_{2,x} W \cos^3 \theta - 2r^2 G_{2,x} W \sin^2 \theta \cos \theta), \\ \sigma_y^D d\sigma_x^R &= (G_{2,x} \cos \theta - r^2 G_{2,y} W \cos \theta \sin^2 \theta) (-G_{1,x} \sin \theta - r^2 G_{1,y} W \sin^3 \theta + 2r^2 G_{1,y} W \cos^2 \theta \sin \theta). \end{aligned}$$

Then we have

$$\sigma_x^R d\sigma_y^D + \sigma_x^D d\sigma_y^R - \sigma_y^R d\sigma_x^D - \sigma_y^D d\sigma_x^R = -\frac{1}{2} r^2 W (\sin 4\theta) (G_{2,x} G_{1,y} + G_{2,y} G_{1,x}).$$

It is straightforward to obtain

$$q = \frac{1}{2\pi} \int_0^{2\pi} d\theta \frac{(G_{1,x} G_{1,y} - G_{2,y} G_{2,x})}{(G_{1,x} \cos \theta + G_{2,y} \sin \theta)^2 + (G_{1,y} \sin \theta + G_{2,x} \cos \theta)^2} - \frac{1}{2\pi} \int_0^{2\pi} d\theta \frac{r^2 W \cos(2\theta)}{(1 + r^4 W^2 \cos^2 \theta \sin^2 \theta)}.$$

The elliptic effect gives the same integral in any case of calculating the topological charge, which is zero. The topological charge is

$$q = \frac{1}{\pi} \int_0^\pi \frac{G_{1,x} G_{1,y} - G_{2,x} G_{2,y}}{A + B \cos t} dt = \frac{G_{1,x} G_{1,y} - G_{2,x} G_{2,y}}{\sqrt{(G_{1,x} G_{1,y} - G_{2,x} G_{2,y})^2}},$$

where

$$\begin{aligned}
 A &= \frac{1}{2}G_{1,x}^2 + \frac{1}{2}G_{2,x}^2 + \frac{1}{2}G_{1,y}^2 + \frac{1}{2}G_{2,y}^2, \\
 B &= \sqrt{\frac{1}{4}(G_{1,x}^2 + G_{2,x}^2 - G_{1,y}^2 - G_{2,y}^2)^2 + (G_{1,x}G_{2,y} + G_{2,x}G_{1,y})^2} \\
 A^2 - B^2 &= (G_{1,x}G_{1,y} - G_{2,x}G_{2,y})^2.
 \end{aligned}$$

Finally, we obtain that the topological charge is equivalent to Eq. (24).

- * Electronic address: Tapash.Chakraborty@umanitoba.ca
- ¹ N. Nagaosa and Y. Tokura, *Nature Nanotech.* **8**, 899 (2013).
 - ² M. Z. Hasan, and C. L. Kane, *Rev. Mod. Phys.* **82**, 3045 (2010).
 - ³ X. L. Qi and S. C. Zhang, *Rev. Mod. Phys.* **83**, 1057 (2011).
 - ⁴ S. Mühlbauer, B. Binz, F. Jonietz, C. Pfleiderer, A. Rosch, A. Neubauer, R. Georgii, P. Böni, *Science* **323**, 915-919 (2009).
 - ⁵ X. Z. Yu, Y. Onose, N. Kanazawa, J. H. Park, J. H. Han, Y. Matsui, N. Nagaosa, and Y. Tokura, *Nature* **465**, 901-904 (2010).
 - ⁶ Z. F. Ezawa, *Quantum Hall Effects: Field Theoretical Approach and Related Topics* (World Scientific, 2000).
 - ⁷ R. Côté, Wenchen Luo, Branko Petrov, Yafis Barlas, and A. H. MacDonald, *Phys. Rev. B* **82**, 245307 (2010); R. Côté, J. P. Fouquet, and Wenchen Luo, *Phys. Rev. B* **84**, 235301 (2011).
 - ⁸ Jiyong Fu, Poliana H. Penteado, Marco O. Hachiya, Daniel Loss, and J.C. Egues, *Phys. Rev. Lett.* **117**, 226401 (2016).
 - ⁹ I. Zutic, J. Fabian, and S. Das Sarma, *Rev. Mod. Phys.* **76**, 323 (2004).
 - ¹⁰ L. Smejkal, Y. Mokrousov, Binghai Yan, and A. H. MacDonald, *Nat. Phys.* **14**, 242 (2018).
 - ¹¹ O. Gomonay, T. Jungwirth, and J. Sinova, *Phys. Stat. Sol. RRL* **11**, 1700022 (2017).
 - ¹² Wenchen Luo, Amin Naseri, Jesko Sirker, and T. Chakraborty, *Sci. Rep.* **9**, 672 (2019).
 - ¹³ P.A. Maksym, and T. Chakraborty, *Phys. Rev. Lett.* **65**, 108 (1990).
 - ¹⁴ T. Chakraborty, *Quantum Dots* (Elsevier, Amsterdam 1999).
 - ¹⁵ D. Bimberg, M. Grundmann, and N. N. Ledentsov, *Quantum Dot Heterostructures* (John Wiley and Sons, Chichester, 1999).
 - ¹⁶ L. P. Kouwenhoven, D. G. Austing, and S. Tarucha, *Rep. Prog. Phys.* **64**, 701-736 (2001).
 - ¹⁷ R. Hanson, L. P. Kouwenhoven, J. R. Petta, S. Tarucha, and L. M. K. Vandersypen, *Rev. Mod. Phys.* **79**, 1217 (2007).
 - ¹⁸ C. Kloeffer, and D. Loss, *Annu. Rev. Condens. Matter Phys.* **4**, 51 (2013).
 - ¹⁹ O. Voskoboynikov, C. P. Lee, and O. Tretyak, *Phys. Rev. B* **63**, 165306 (2001).
 - ²⁰ M. Governale, *Phys. Rev. Lett.* **89**, 206802 (2002).
 - ²¹ A. Emperador, E. Lipparini, and F. Pederiva, *Phys. Rev. B* **70**, 125302 (2004).
 - ²² D. V. Bulaev, and D. Loss, *Phys. Rev. B* **71**, (2005).
 - ²³ S. Weiss and R. Egger, *Phys. Rev. B* **72**, 245301 (2005).
 - ²⁴ T. Chakraborty, and P. Pietiläinen, *Phys. Rev. Lett.* **95**, 136603 (2005); P. Pietiläinen, and T. Chakraborty, *Phys. Rev. B* **73**, 155315 (2006).
 - ²⁵ A. Ambrosetti, F. Pederiva, and E. Lipparini, *Phys. Rev. B* **83**, 155301 (2011).
 - ²⁶ C. F. Destefani, S. E. Ulloa, and G. E. Marques, *Phys. Rev. B* **69**, 125302 (2004).
 - ²⁷ T. Chakraborty, and P. Pietiläinen, *Phys. Rev. B* **71**, 113305 (2005).
 - ²⁸ A. Cavalli, F. Malet, J. C. Cremon, and S. M. Reimann, *Phys. Rev. B* **84**, 235117 (2011).
 - ²⁹ A. Naseri, A. Zazunov, and R. Egger, *Phys. Rev. X* **4**, 031033 (2014).
 - ³⁰ E. Tsitsishvili, G. S. Lozano, and A. O. Gogolin, *Phys. Rev. B* **70**, 115316 (2004).
 - ³¹ S. K. Ghosh, Jayantha P. Vyasankere, and V. B. Shenoy, *Phys. Rev. A* **84**, 053629 (2011).
 - ³² Yi Li, Xiangfa Zhou, and Congjun Wu, *Phys. Rev. B* **85**, 125122 (2012).
 - ³³ S. Avetisyan, Pekka Pietiläinen, and Tapash Chakraborty, *Phys. Rev. B* **88**, 205310 (2013).
 - ³⁴ S. D. Ganichev, V. V. Bel'kov, L. E. Golub, E. L. Ivchenko, Petra Schneider, S. Giglberger, J. Eroms, J. De Boeck, G. Borghs, W. Wegscheider, D. Weiss, and W. Prettl, *Phys. Rev. Lett.* **92**, 256601 (2004).
 - ³⁵ C. J. Stevenson, J. Kyriakidis, *Phys. Rev. B* **84**, 075303 (2011).
 - ³⁶ G. A. Intronati, P. I. Tamborenea, D. Weinmann, R. A. Jalabert, *Phys. Rev. B* **88**, 045303 (2013).
 - ³⁷ D. Pfannkuche and R.R. Gerhardt, *Phys. Rev. B* **44**, 13132 (1991).
 - ³⁸ D. Pfannkuche, V. Gudmundsson, and P.A. Maksym, *Phys. Rev. B* **47**, 2244 (1993).
 - ³⁹ J. Nitta, T. Akazaki, H. Takayanagi, and T. Enoki, *Phys. Rev. Lett.* **78**, 1335 (1997).
 - ⁴⁰ M. Kohda, T. Bergsten, and J. Nitta, *J. Phys. Soc. Jpn.* **77**, 031008 (2008).
 - ⁴¹ C. R. Ast, D. Pacilé, L. Moreschini, M. C. Falub, M. Pagnano, K. Kern, M. Grioni, J. Henk, A. Ernst, S. Ostanin, and P. Bruno, *Phys. Rev. B* **77**, 081407(R) (2008).
 - ⁴² Y. Kanai, R. S. Deacon, S. Takahashi, A. Oiwa, K. Yoshida, K. Shibata, K. Hirakawa, Y. Tokura, and S. Tarucha, *Nat. Nanotechnol.* **6**, 511 (2011).
 - ⁴³ M. P. Nowak, B. Szafran, F. M. Peeters, B. Partoens, and W. J. Pasek, *Phys. Rev. B* **83**, 245324 (2011).

- ⁴⁴ C. L. Yang, Junfeng Dai, W. K. Ge, Xiaodong Cui, Appl. Phys. Lett. **96**, 152109 (2010); A. Srinivasan, K. L. Hudson, D. Miserev, L. A. Yeoh, O. Klochan, K. Muraki, Y. Hirayama, O. P. Sushkov, and A. R. Hamilton Phys. Rev. B **94**, 041406(R) (2016).
- ⁴⁵ J. Mannhart, D.H.A. Blank, H.Y. Hwang, A.J. Millis, J.-M. Triscone, MRS Bulletin **33**, 1027 (2008); J. Mannhart, D.G. Schlom, Science **327**, 1607 (2010); Z.L. Wang, Mater. Today **7**, 26 (2004).
- ⁴⁶ J. Falson, D. Maryenko, B. Friess, D. Zhang, Y. Kozuka, A. Tsukazaki, J.H. Smet, M. Kawasaki, Nat. Phys. **11**, 347 (2015).
- ⁴⁷ Joseph Falson, Daniela Tabrea, Ding Zhang, Inti Sodemann, Yusuke Kozuka, Atsushi Tsukazaki, Masashi Kawasaki, Klaus von Klitzing and Jurgen H. Smet, Sci. Adv. **4**: eaat8742 (2018).
- ⁴⁸ W. Luo, T. Chakraborty, Phys. Rev. B **93**, 161103(R) (2016); Phys. Rev. B **94**, 161101(R) (2016); Phys. Rev. B **96**, 081108(R) (2017).
- ⁴⁹ T. Chakraborty, A. Manaselyan, and M. Barseghyan, J. Phys.:Condens. Matter **29**, 215301 (2017).
- ⁵⁰ T. Chakraborty, A. Manaselyan, and M. Berseghyan, in *Physics of Quantum Rings* (Springer, Berlin 2018), edited by V.M. Fomin.
- ⁵¹ A.E. Dementyev, P. Khandelwal, N. N. Kuzma, S.E. Barrett, L. N. Pfeiffer, K. W. West, Solid State Comm. **119**, 217 (2001); N. N. Kuzma, P. Khandelwal, S. E. Barrett, L. N. Pfeiffer, K. W. West, Science **281**, 686 (1998); S. E. Barrett, G. Dabbagh, L. N. Pfeiffer, K. W. West, and R. Tycko, Phys. Rev. Lett. **74**, 5112 (1995).